Milky Way Satellite Census. III. Constraints on Dark Matter Properties from Observations of Milky Way Satellite Galaxies

Preprint · July 2020

68 authors, including:

Keith Bechtol
University of Chicago

Risa Wechsler
Stanford University

Vera Gluscevic
Institute for Advanced Study

Juan Garcia-Bellido
Universidad Autónoma de Madrid

DES-2020-546, FERMILAB-PUB-20-277-AE, SLAC-PUB-17554

Milky Way Satellite Census. III. Constraints on Dark Matter Properties from Observations of Milky Way Satellite Galaxies

E. O. Nadler,[1,2,3,*] A. Drlica-Wagner,[4,5,6,†] K. Bechtol,[7] S. Mau,[5] R. H. Wechsler,[1,2,3] V. Gluscevic,[8] K. Boddy,[9] A. B. Pace,[10] T. S. Li,[11,12,‡] M. McNanna,[7] A. H. Riley,[13] J. García-Bellido,[14] Y.-Y. Mao,[15,‡] G. Green,[16] D. L. Burke,[2,3] A. Peter,[17,18,19] B. Jain,[20] T. M. C. Abbott,[21] M. Aguena,[22,23] S. Allam,[4] J. Annis,[4] S. Avila,[14] D. Brooks,[24] M. Carrasco Kind,[25,26] J. Carretero,[27] M. Costanzi,[28,29] L. N. da Costa,[23,30] J. De Vicente,[31] S. Desai,[32] H. T. Diehl,[4] P. Doel,[24] S. Everett,[33] A. E. Evrard,[34,35] B. Flaugher,[4] J. Frieman,[4,5] D. W. Gerdes,[34,35] D. Gruen,[1,2,3] R. A. Gruendl,[25,26] J. Gschwend,[23,30] G. Gutierrez,[4] S. R. Hinton,[36] K. Honscheid,[19,17] D. Huterer,[35] D. J. James,[37] E. Krause,[38] K. Kuehn,[39,40] N. Kuropatkin,[4] O. Lahav,[24] M. A. G. Maia,[23,30] J. L. Marshall,[13] F. Menanteau,[25,26] R. Miquel,[41,27] A. Palmese,[4,5] F. Paz-Chinchón,[42,26] A. A. Plazas,[11] A. K. Romer,[43] E. Sanchez,[31] V. Scarpine,[4] S. Serrano,[44,45] I. Sevilla-Noarbe,[31] M. Smith,[46] M. Soares-Santos,[47] E. Suchyta,[48] M. E. C. Swanson,[26] G. Tarle,[35] D. L. Tucker,[4] A. R. Walker,[21] and W. Wester[4]

(DES Collaboration)

[1] *Department of Physics, Stanford University, 382 Via Pueblo Mall, Stanford, CA 94305, USA*
[2] *Kavli Institute for Particle Astrophysics & Cosmology, P. O. Box 2450, Stanford University, Stanford, CA 94305, USA*
[3] *SLAC National Accelerator Laboratory, Menlo Park, CA 94025, USA*
[4] *Fermi National Accelerator Laboratory, P. O. Box 500, Batavia, IL 60510, USA*
[5] *Kavli Institute for Cosmological Physics, University of Chicago, Chicago, IL 60637, USA*
[6] *Department of Astronomy and Astrophysics, University of Chicago, Chicago, IL 60637, USA*
[7] *Physics Department, 2320 Chamberlin Hall, University of Wisconsin-Madison, 1150 University Avenue Madison, WI 53706-1390*
[8] *University of Southern California. Department of Physics and Astronomy, 825 Bloom Walk ACB 439. Los Angeles, CA 90089-0484, USA*
[9] *Department of Physics & Astronomy, Johns Hopkins University, Baltimore, MD 21218, USA, USA*
[10] *Department of Physics, Carnegie Mellon University, Pittsburgh, Pennsylvania 15312, USA*
[11] *Department of Astrophysical Sciences, Princeton University, Peyton Hall, Princeton, NJ 08544, USA*
[12] *Observatories of the Carnegie Institution for Science, 813 Santa Barbara St., Pasadena, CA 91101, USA*
[13] *George P. and Cynthia Woods Mitchell Institute for Fundamental Physics and Astronomy, and Department of Physics and Astronomy, Texas A&M University, College Station, TX 77843, USA*
[14] *Instituto de Fisica Teorica UAM/CSIC, Universidad Autonoma de Madrid, 28049 Madrid, Spain*
[15] *Department of Physics and Astronomy, Rutgers, The State University of New Jersey, Piscataway, NJ 08854, USA*
[16] *Max Planck Institute for Astronomy, Königstuhl 17 D-69117, Heidelberg, Germany*
[17] *Department of Physics, The Ohio State University, Columbus, OH 43210, USA*
[18] *Department of Astronomy, The Ohio State University, Columbus, OH 43210, USA*
[19] *Center for Cosmology and Astro-Particle Physics, The Ohio State University, Columbus, OH 43210, USA*
[20] *Department of Physics and Astronomy, University of Pennsylvania, Philadelphia, PA 19104, USA*
[21] *Cerro Tololo Inter-American Observatory, NSF's National Optical-Infrared Astronomy Research Laboratory, Casilla 603, La Serena, Chile*
[22] *Departamento de Física Matemática, Instituto de Física, Universidade de São Paulo, CP 66318, São Paulo, SP, 05314-970, Brazil*
[23] *Laboratório Interinstitucional de e-Astronomia - LIneA, Rua Gal. José Cristino 77, Rio de Janeiro, RJ - 20921-400, Brazil*
[24] *Department of Physics & Astronomy, University College London, Gower Street, London, WC1E 6BT, UK*
[25] *Department of Astronomy, University of Illinois at Urbana-Champaign, 1002 W. Green Street, Urbana, IL 61801, USA*
[26] *National Center for Supercomputing Applications, 1205 West Clark St., Urbana, IL 61801, USA*
[27] *Institut de Física d'Altes Energies (IFAE), The Barcelona Institute of Science and Technology, Campus UAB, 08193 Bellaterra (Barcelona) Spain*
[28] *INAF-Osservatorio Astronomico di Trieste, via G. B. Tiepolo 11, I-34143 Trieste, Italy*
[29] *Institute for Fundamental Physics of the Universe, Via Beirut 2, 34014 Trieste, Italy*
[30] *Observatório Nacional, Rua Gal. José Cristino 77, Rio de Janeiro, RJ - 20921-400, Brazil*
[31] *Centro de Investigaciones Energéticas, Medioambientales y Tecnológicas (CIEMAT), Madrid, Spain*
[32] *Department of Physics, IIT Hyderabad, Kandi, Telangana 502285, India*
[33] *Santa Cruz Institute for Particle Physics, Santa Cruz, CA 95064, USA*
[34] *Department of Astronomy, University of Michigan, Ann Arbor, MI 48109, USA*
[35] *Department of Physics, University of Michigan, Ann Arbor, MI 48109, USA*

[36] School of Mathematics and Physics, University of Queensland, Brisbane, QLD 4072, Australia
[37] Center for Astrophysics | Harvard & Smithsonian, 60 Garden Street, Cambridge, MA 02138, USA
[38] Department of Astronomy/Steward Observatory, University of Arizona, 933 North Cherry Avenue, Tucson, AZ 85721-0065, USA
[39] Australian Astronomical Optics, Macquarie University, North Ryde, NSW 2113, Australia
[40] Lowell Observatory, 1400 Mars Hill Rd, Flagstaff, AZ 86001, USA
[41] Institució Catalana de Recerca i Estudis Avançats, E-08010 Barcelona, Spain
[42] Institute of Astronomy, University of Cambridge, Madingley Road, Cambridge CB3 0HA, UK
[43] Department of Physics and Astronomy, Pevensey Building, University of Sussex, Brighton, BN1 9QH, UK
[44] Institut d'Estudis Espacials de Catalunya (IEEC), 08034 Barcelona, Spain
[45] Institute of Space Sciences (ICE, CSIC), Campus UAB, Carrer de Can Magrans, s/n, 08193 Barcelona, Spain
[46] School of Physics and Astronomy, University of Southampton, Southampton, SO17 1BJ, UK
[47] Brandeis University, Physics Department, 415 South Street, Waltham MA 02453
[48] Computer Science and Mathematics Division, Oak Ridge National Laboratory, Oak Ridge, TN 37831
(Dated: August 4, 2020)

We perform a comprehensive study of Milky Way (MW) satellite galaxies to constrain the fundamental properties of dark matter (DM). This analysis fully incorporates inhomogeneities in the spatial distribution and detectability of MW satellites, and marginalizes over uncertainties in the mapping between galaxies and DM halos, the properties of the MW system, and the disruption of subhalos by the MW disk. Our results are consistent with the cold, collisionless DM paradigm and yield the strongest cosmological constraints to date on particle models of warm, interacting, and fuzzy dark matter. At 95% confidence, we report limits on (*i*) the mass of thermal relic warm DM, $m_{\rm WDM} > 6.5\,\rm keV$ (free-streaming length, $\lambda_{\rm fs} \lesssim 10\,h^{-1}\,\rm kpc$), (*ii*) the velocity-independent DM–proton scattering cross section, $\sigma_0 < 8.8 \times 10^{-29}\,\rm cm^2$ for a 100 MeV DM particle mass (DM–proton coupling, $c_p \lesssim (0.3\,\rm GeV)^{-2}$), and (*iii*) the mass of fuzzy DM, $m_\phi > 2.9 \times 10^{-21}\,\rm eV$ (de Broglie wavelength, $\lambda_{\rm dB} \lesssim 0.5\,\rm kpc$). These constraints are complementary to other observational and laboratory constraints on DM properties.

PACS numbers: 95.35.+d, 95.85.Pw, 98.52.Wz
Keywords: dark matter, Galaxy: halo, galaxies: dwarf

Introduction.—In the concordance model of cosmology, collisionless cold dark matter (CDM) makes up $\sim 25\%$ of the matter–energy density of the Universe [1]. While dark matter (DM) has the potential to solve a number of outstanding challenges in the Standard Model (SM) of particle physics [2–4], the only positive empirical evidence for DM comes from cosmological and astrophysical observations. Furthermore, by studying the astrophysical distribution of DM, it is possible to probe its particle nature [5, 6]. Specifically, the formation, abundance, and structure of gravitationally bound DM structures, known as "halos," provide valuable information about viable ranges of the DM particle mass, production mechanism, and couplings to the SM. In particular, the abundance and properties of the smallest DM halos have the potential to indicate a departure from the CDM paradigm [5, 6].

The smallest known DM halos host the ultra-faint dwarf satellite galaxies of the Milky Way (MW) [7]. In these systems, star formation is highly suppressed by reionization and stellar feedback, leading to mass-to-light ratios that are hundreds of times larger than the universal average [7, 8]. Ultra-faint satellite galaxies are thus pristine laboratories for studying DM; in particular, the abundance of these systems is a sensitive probe of *any* DM physics that suppresses the formation or present-day abundance of small halos.

In particular, the following theoretical paradigms for DM affect the properties of the MW satellite population:

(*i*) *Warm dark matter (WDM)* is produced in the early Universe with a temperature of $\mathcal{O}(1\,\rm keV)$, although its momentum distribution can be non-thermal. Any viable WDM candidate must be cold enough to reproduce the observed large-scale structure, but its non-negligible free-streaming length suppresses the formation of the low-mass halos that host MW satellite galaxies [9–14]. One of the most popular WDM candidates is a sterile neutrino [15, 16].

(*ii*) *Interacting dark matter (IDM)* couples strongly enough to the SM to be heated by interactions with the photon–baryon fluid before recombination. This collisional damping washes out small-scale structure, even if the DM is produced non-thermally [17–19]. DM–nucleon interactions arise in generalizations of the weakly-interacting-massive-particle (WIMP) scenario [20–22], and the impact of DM–radiation interactions on low-mass halos has also been studied [23–25]. Here, we consider a velocity- and spin-independent DM–proton coupling, c_p.

(*iii*) *Fuzzy dark matter (FDM)* consists of an ultra-light boson with a sufficiently small mass, $\mathcal{O}(10^{-22}\,\rm eV)$, such that its de Broglie wavelength is comparable to the sizes of dwarf galaxies, $\mathcal{O}(1\,\rm kpc)$; this inhibits the formation of low-mass halos due to the uncertainty principle [26–28]. Ultra-light axions constitute one popular class of FDM [29].

In this *Letter*, we use novel measurements and modeling of the MW satellite galaxy population to constrain each DM paradigm described above. Specifically, we combine a census of MW satellites [30] from the Dark Energy Survey (DES; [31]) and Pan-STARRS1 (PS1; [32]) with a rigorous forward-modeling framework [33] to fit the position-dependent MW satellite luminosity function in each of these DM paradigms. This procedure fully incorporates inhomogeneities in the observed MW satellite population and marginalizes over uncertainties in the mapping between MW satellite galaxies and DM halos, the efficiency of subhalo disruption due to the MW disk, and the properties of the MW system.

Our analysis yields stringent constraints on each DM paradigm based on the abundance of observed MW satellites. These limits are complementary to constraints from the Lyman-α forest [34–36], strongly-lensed systems [37, 38], and MW stellar streams [39]. Our results imply that CDM is consistent with astrophysical observations down to the smallest currently accessible scales ($k \sim 40\,h\,\mathrm{Mpc}^{-1}$) and strongly reinforce previous work demonstrating that there is no "missing satellites problem" in the MW [40]. Throughout this work, we fix cosmological parameters at $h = 0.7$, $\Omega_\mathrm{m} = 0.286$, $\Omega_\Lambda = 0.714$, $\sigma_8 = 0.82$, $n_s = 0.96$ [41].

Analysis Overview.—Our procedure is based on [19] with several specific improvements for each DM paradigm under consideration. Before discussing each DM paradigm in detail, we describe the main components of our analysis used to connect non-CDM scenarios to the observed MW satellite population. For each paradigm, we assume that the non-CDM component constitutes the entirety of the DM.

Transfer function. The linear matter power spectrum, normalized to that of CDM, is used to generate initial conditions for simulations of structure formation. In particular, the transfer function is defined as

$$T^2(k) \equiv \frac{P_\mathrm{DM}(k)}{P_\mathrm{CDM}(k)}, \tag{1}$$

where k is the cosmological wavenumber, $P_\mathrm{CDM}(k)$ is the CDM linear matter power spectrum, and $P_\mathrm{DM}(k)$ is the linear matter power spectrum of a non-CDM model [42]. $P_\mathrm{DM}(k)$ is obtained by integrating the relevant Boltzmann equation (which may include DM–SM interactions) given the initial DM phase-space distribution. The left panel of Fig. 1 illustrates the transfer function for the three DM paradigms we consider.

It is convenient to define the *half-mode scale*, k_hm, as the wavenumber satisfying $T^2(k_\mathrm{hm}) = 0.25$ [43]. The corresponding *half-mode mass*,

$$M_\mathrm{hm} = \frac{4\pi}{3}\Omega_\mathrm{m}\bar{\rho}\left(\frac{\pi}{k_\mathrm{hm}}\right)^3, \tag{2}$$

is a characteristic mass scale below which the abundance of DM halos is significantly suppressed relative to CDM. Here, $\bar{\rho}$ is the critical density of the Universe today.

Subhalo mass function (SHMF). The abundance of subhalos within the virial radius of the MW is expressed as the cumulative number of subhalos as a function of subhalo mass, M. We follow [19] by using peak virial mass, defined according to the Bryan-Norman overdensity [44] with $\Delta_\mathrm{vir} \simeq 99.2$ (consistent with our cosmological parameters). We define

$$\left(\frac{\mathrm{d}N_\mathrm{sub}}{\mathrm{d}M}\right)_\mathrm{DM} \equiv f_\mathrm{DM}(M, \boldsymbol{\theta}_\mathrm{DM})\left(\frac{\mathrm{d}N_\mathrm{sub}}{\mathrm{d}M}\right)_\mathrm{CDM}, \tag{3}$$

where $f_\mathrm{DM}(M, \boldsymbol{\theta}_\mathrm{DM})$ is the suppression of the SHMF relative to CDM and $\boldsymbol{\theta}_\mathrm{DM}$ are DM model parameters; both f_DM and $\boldsymbol{\theta}_\mathrm{DM}$ depend on the DM model in question. The middle panel of Fig. 1 shows SHMF suppression for the three DM paradigms we consider.

MW satellite model. We combine the SHMF suppression in Eq. (3) with the modeling framework from [33] to predict the abundance of observed MW satellites in each DM paradigm. This modeling framework combines cosmological zoom-in simulations [45]—which are chosen to match the inferred mass, concentration, and assembly history of the MW halo and include realistic analogs of the Large Magellanic Cloud system—with a statistical model of the galaxy–halo connection in order to populate subhalos with satellite galaxies.

We implement SHMF suppression by multiplying the detection probability of each mock satellite, which includes terms that model tidal disruption due to the MW disk, the efficiency of galaxy formation, and observational detectability, by a factor of $f_\mathrm{DM}(M, \boldsymbol{\theta}_\mathrm{DM})$, following [19, 46]. This procedure assumes that the shape of the observed radial satellite distribution (which our model predicts reasonably well; [33]) is unchanged in alternative DM scenarios, which is consistent with results from cosmological WDM simulations of MW-mass halos [47, 48]. The validity of this assumption is less certain for FDM because dynamical friction operates differently for wave-like versus particle DM, although this difference is expected to be negligible for the $\sim 10^8\,\mathrm{M}_\odot$ subhalos that drive our constraints [49]. The right panel of Fig. 1 shows the predicted satellite luminosity function for each DM model under consideration.

Fitting procedure. We fit predicted satellite populations to the observed satellite population from DES and PS1 using the observational selection functions derived in [30], assuming that satellite surface brightness is distributed according to a Poisson point process in each survey footprint [33, 50]. We use the Markov Chain Monte

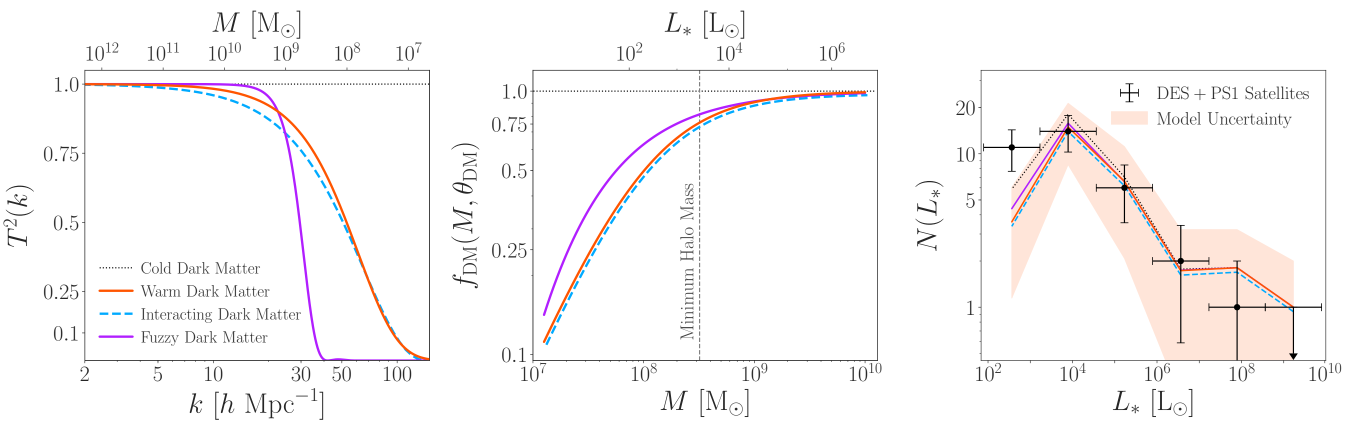

FIG. 1. *Left panel*: Transfer functions for the WDM (orange), IDM (blue), and FDM (magenta) paradigms, evaluated at our fiducial 95% confidence constraints of $m_{\rm WDM} = 6.5\,{\rm keV}$, $\sigma_0 = 8.8 \times 10^{-29}\,{\rm cm}^2$ (for DM particle mass $m_\chi = 100\,{\rm MeV}$), and $m_\phi = 2.9 \times 10^{-21}\,{\rm eV}$, respectively. These constraints are marginalized over our MW satellite model and the properties of the MW system. *Middle panel*: SHMF suppression relative to CDM for each DM model. The vertical dashed line indicates the 95% confidence upper limit on the lowest-mass halo inferred to host MW satellite galaxies [33]. Note that the IDM SHMF is assumed to be identical to the WDM SHMF in our analysis, and is offset slightly for visual clarity. *Right panel*: Predicted MW satellite galaxy luminosity functions for each DM model compared to DES and PS1 observations, evaluated at the best-fit MW satellite model parameters from [33]. The shaded band illustrates the uncertainty of our WDM prediction due to the stochasticity of our galaxy–halo connection model and the limited number of simulations used in our analysis; the size of this uncertainty is very similar to that in CDM and the other alternative DM models shown. This panel is a simple one-dimensional representation of our multidimensional MW satellite and DM model fit to the luminosity, size, and spatial distribution of satellites in the DES and PS1 survey footprints as described in [33]; full posterior distributions are provided in the Supplemental Material.

Carlo (MCMC) code `emcee` [51] to simultaneously fit for seven parameters governing the galaxy–halo connection, one parameter governing the impact of the MW disk on subhalo disruption, and one parameter governing the impact of the DM model in question, which we express as a subhalo mass scale. In particular, our thermal relic WDM constraint is derived by fitting for $M_{\rm hm}$, and our FDM limit is derived by fitting for a characteristic mass scale M_0. Further details on our fitting procedure are provided in the Supplemental Material.

Subhalo abundance is known to scale linearly with host halo mass [45], and we assume that satellite luminosity is a monotonic function of subhalo mass, modulo scatter [33]. We therefore expect a higher-mass MW host halo to yield weaker constraints on non-CDM models, because observed satellites would inhabit correspondingly higher-mass subhalos. The average virial mass of our simulated MW-like halos is $1.4 \times 10^{12}\,{\rm M}_\odot$, which is consistent with the 95% confidence range for the virial mass of the MW halo inferred from *Gaia* measurements of satellite kinematics, i.e. $1.0 \times 10^{12}\,{\rm M}_\odot < M_{\rm MW} < 1.8 \times 10^{12}\,{\rm M}_\odot$ [52]. To be conservative, we account for the uncertainty in MW halo mass on our DM constraints by assuming that the mass scale describing the suppression of the SHMF in each DM paradigm is linearly related to the virial mass of the MW halo, following the scaling for minimum halo mass derived in [33]. In particular, we multiply the upper limit on the characteristic mass scale in each of our non-CDM fits by the ratio of the largest allowed MW halo mass to the average host halo mass in our simulations. We validate this procedure by fitting the observed satellite population using each MW-like simulation separately, which yields reasonable agreement with the linear scaling expectation.

In summary, our fit to the MW satellite population incorporates both intrinsic inhomogeneities in the spatial distribution of MW satellites and those introduced by the varying coverage and depth of current surveys. We assume that alternative DM physics only modifies the SHMF, via Eq. (3), and we report 95% confidence limits on DM model parameters that are marginalized over uncertainties in our MW satellite model and the properties of the MW system.

WDM Analysis. Thermal relic WDM with particle mass, $m_{\rm WDM}$, has been studied extensively in the literature (e.g., [13, 53]) and serves as a benchmark model.

Transfer function. The transfer function for thermal relic WDM is given as a function of $m_{\rm WDM}$ by [53]. This transfer function is commonly assumed in cosmological studies of WDM and facilitates a well-defined comparison to other small-scale structure results [34, 35, 37–39]. However, the simple thermal relic transfer function is inadequate to describe specific particle models of WDM, such as resonantly-produced sterile neutrinos [54]. Thus, constraints on specific DM candidates must be inferred using transfer functions appropriate for the particle model in question, as we discuss below.

SHMF. Several authors have implemented the thermal

Dark Matter Paradigm	Parameter	Constraint	Derived Property	Constraint
Warm Dark Matter	Thermal Relic Mass	$m_{\mathrm{WDM}} > 6.5\,\mathrm{keV}$	Free-streaming Length	$\lambda_{\mathrm{fs}} \lesssim 10\,h^{-1}\,\mathrm{kpc}$
Interacting Dark Matter	Velocity-independent DM–Proton Cross Section	$\sigma_0 < 8.8 \times 10^{-29}\,\mathrm{cm}^2$	DM–Proton Coupling	$c_p \lesssim (0.3\,\mathrm{GeV})^{-2}$
Fuzzy Dark Matter	Particle Mass	$m_\phi > 2.9 \times 10^{-21}\,\mathrm{eV}$	de Broglie Wavelength	$\lambda_{\mathrm{dB}} \lesssim 0.5\,\mathrm{kpc}$

TABLE I. Constraints on the WDM, IDM, and FDM paradigms from observations of MW satellite galaxies. Limits for each non-CDM model are derived by assuming that it constitutes the entirety of the DM. The first column lists the DM paradigm, the second column describes the particle physics parameters constrained by this analysis, the third column lists the corresponding constraints at 95% confidence, the fourth column describes the derived property constrained for each DM model, and the fifth column lists constraints on the derived parameters. Limits on the DM–proton scattering cross sections depend on the DM particle mass, m_χ (see Fig. 2); for simplicity, we present our constraint for $m_\chi = 100\,\mathrm{MeV}$.

relic WDM transfer function from [53] in cosmological zoom-in simulations to estimate the suppression of the SHMF in MW-mass host halos [13, 43, 48, 55]. These results depend on the algorithm used to remove spurious halos [55, 56], and therefore vary among studies. Following [57], SHMF suppression for thermal relic WDM can be expressed as

$$f_{\mathrm{WDM}}(M, m_{\mathrm{WDM}}) = \left[1 + \left(\frac{\alpha M_{\mathrm{hm}}(m_{\mathrm{WDM}})}{M}\right)^{\beta}\right]^{\gamma}, \quad (4)$$

where α, β, and γ are constants, and M_{hm} is related to m_{WDM} in our fiducial cosmology via

$$M_{\mathrm{hm}}(m_{\mathrm{WDM}}) = 5 \times 10^8 \left(\frac{m_{\mathrm{WDM}}}{3\,\mathrm{keV}}\right)^{-10/3} \mathrm{M}_\odot. \quad (5)$$

To facilitate comparison with recent WDM constraints from analyses of the MW satellite population [19], strong gravitational lenses [37, 38], and stellar streams [39], we adopt the SHMF from [13], which corresponds to Eq. (4) with $\alpha = 2.7$, $\beta = 1.0$, and $\gamma = -0.99$. We note that the recent estimate of the SHMF from [57]—which specifically models resonantly-produced sterile neutrino WDM—is significantly *less* suppressed than the thermal relic SHMF from [13]. Thus, our fiducial WDM constraint only applies directly to thermal relic DM.

Fitting procedure. We implement Eq. (4) in our fit to the MW satellite population to obtain a marginalized posterior distribution over M_{hm}. In particular, we fit for $\log_{10}(M_{\mathrm{hm}})$ using a uniform prior on this logarithmic quantity, and we translate the resulting limit to m_{WDM} using Eq. (5). We translate our thermal relic WDM limit into constraints on resonantly-produced sterile neutrinos by following [58, 59]. Specifically, we analyze sterile neutrino transfer functions over a grid of mass and mixing angle values [60], and we constrain sterile neutrino models that produce transfer functions which are strictly more suppressed than our 95% confidence ruled-out thermal relic WDM model. This procedure is described in detail in the Supplemental Material.

IDM Analysis. Our treatment of IDM follows the prescription of [19]. For concreteness, we focus on the case of velocity-independent DM–proton scattering.

Transfer function. Following [19], the transfer function in our fiducial IDM model is obtained using the modified version of the Boltzmann solver `CLASS` described in [20–22], which we use to evolve linear cosmological perturbations in the presence of velocity-independent DM–proton interactions. These interactions are described by the velocity-independent scattering cross section, σ_0, and the DM particle mass, m_χ. As noted in [19], transfer functions for this model are very similar to those of thermal relic WDM, modulo dark acoustic oscillations that occur at very small scales and are significantly suppressed for our parameter space of interest.

SHMF. Because cosmological zoom-in simulations including DM–proton scattering have not been performed, we follow [19] by mapping the SHMF suppression of IDM to that of WDM based on the correspondence of the transfer functions. In particular, we match the half-mode scales in the transfer functions to construct a relation between m_{WDM} and (σ_0, m_χ), and we assume that the IDM SHMF is identical to the corresponding thermal relic WDM SHMF from [13]. This procedure neglects late-time DM–proton scattering, which [19] estimated to have a negligible impact on subhalo abundances.

Fitting procedure. Following [19], we use the mapping procedure described above to translate our 95% confidence limit on thermal relic WDM into limits on σ_0 for several values of m_χ in our fiducial IDM model.

FDM Analysis. Finally, we provide details on each step for the FDM paradigm. We focus on the case of ultra-light scalar field DM with negligible self-interactions and SM couplings.

Transfer function. The FDM transfer function is given as a function of the FDM mass, m_ϕ, by [26]. We note that this transfer function features steeper power suppression than thermal relic WDM for a fixed half-mode scale.

SHMF. We assume that the FDM SHMF suppression takes the form of Eq. (3), and we fit the results of the

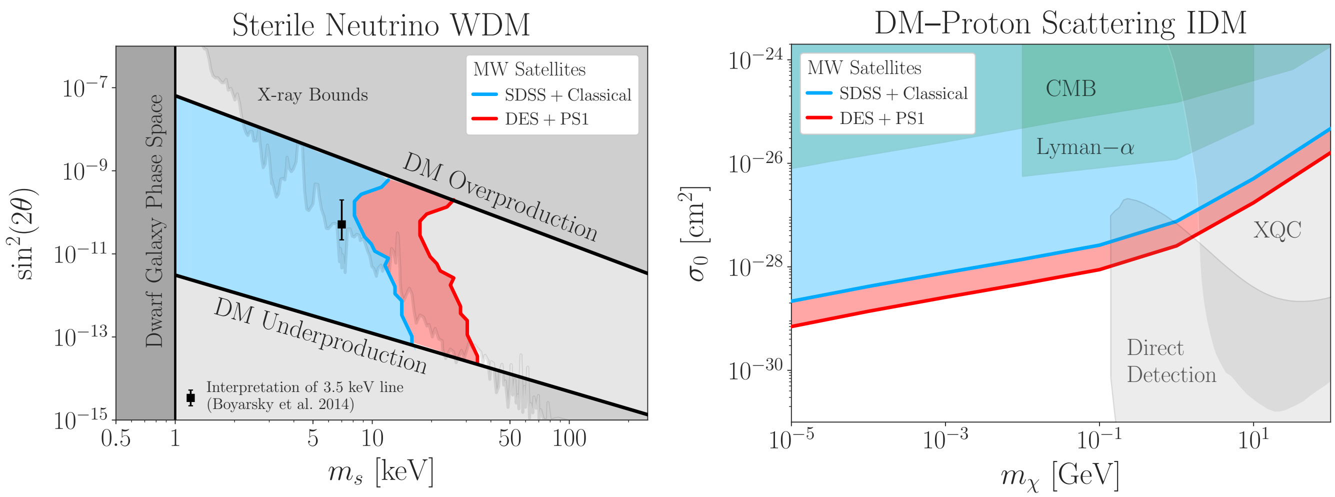

FIG. 2. Constraints on WDM and IDM models from our analysis of MW satellites observed with DES and PS1 (red) compared to previous constraints from classical and SDSS satellites [19] (blue) and other experimental results. *Left panel*: Constraints on the mass and mixing angle of resonantly-produced sterile neutrino DM. These constraints are derived by finding mass and mixing angle combinations that suppress the linear matter power spectrum more strongly than the $m_{\rm WDM} = 6.5\,\rm keV$ thermal relic ruled out at 95% confidence by our analysis. The black point with error bars shows the sterile neutrino interpretation of the 3.5 keV X-ray line [61]. The dark gray region is ruled out by dwarf galaxy internal dynamics [62], and the gray contour shows X-ray constraints [63–65]. Solid black lines indicate regions of parameter space in which resonantly-produced sterile neutrinos cannot constitute all of the DM in the Neutrino Minimal Standard Model [58, 66]. *Right panel*: Constraints on the interaction cross section and DM mass for velocity-independent DM–proton scattering. Green contours show cosmological limits from the CMB [20, 22] and the Lyman-α forest [67]. Light gray contours show experimental limits from the X-ray Quantum Calorimeter [68] and direct detection results as interpreted by [69].

semi-analytic model in [28] with a function of the form,

$$f_{\rm FDM}(M, m_\phi) = \left[1 + \left(\frac{M_0(m_\phi)}{M}\right)^{\tilde{\beta}(m_\phi)}\right]^{\tilde{\gamma}(m_\phi)}, \quad (6)$$

where $\tilde{\beta}(m_\phi)$ and $\tilde{\gamma}(m_\phi)$ are provided in the Supplemental Material. The characteristic subhalo mass scale M_0 is related to the FDM mass via [70]

$$M_0(m_\phi) = 1.6 \times 10^{10} \left(\frac{m_\phi}{10^{-22}\,\rm eV}\right)^{-4/3} \rm M_\odot. \quad (7)$$

The SHMF suppression in Eq. (6) encapsulates the effects of tidal stripping on subhalos with solitonic cores, which was explicitly included by [28]. This SHMF suppression is significantly less severe than that estimated from the FDM simulations in [70]. As described in the Supplemental Material, using the SHMF from [70] in our fit yields a limit on the FDM mass that is roughly three times more stringent than our fiducial result. This confirms that the FDM SHMF is a key theoretical uncertainty that must be addressed [27].

Fitting procedure. We implement the SHMF in Eq. (6) in our fit to the MW satellite population to obtain a marginalized posterior distribution over M_0. In particular, we fit for $\log_{10}(M_0)$ using a uniform prior on this logarithmic quantity, and we translate the resulting limit to m_ϕ using Eq. (7). We note that our procedure for constraining FDM uses the detailed *shape* of the SHMF suppression in this model, rather than mapping the half-mode scale of the FDM transfer function to that of thermal relic WDM as in [19] or bounding the FDM SHMF by ruled-out thermal relic WDM SHMFs as in [71]. This is necessary because both the shape of the FDM transfer function and the resulting suppression of the SHMF differ in detail from thermal relic WDM (see Fig. 1).

Results.—Table I presents our constraints on the WDM, IDM, and FDM paradigms. We describe these results below and translate the limits into constraints on specific models corresponding to each DM paradigm.

(i) *WDM.* Our fit using the thermal relic WDM SHMF suppression from [13] yields $M_{\rm hm} < 3.0 \times 10^7\,\rm M_\odot$, or $m_{\rm WDM} > 7.0\,\rm keV$, at 95% confidence. Linear scaling with MW halo mass yields our fiducial constraint of $M_{\rm hm} < 3.8 \times 10^7\,\rm M_\odot$, corresponding to $m_{\rm WDM} > 6.5\,\rm keV$. This translates to an upper limit on the free-streaming length of $\lambda_{\rm fs} \lesssim 10\ h^{-1}\,\rm kpc$, corresponding to the virial radii of the smallest halos that host MW satellite galaxies, and improves on previous $m_{\rm WDM}$ constraints from the MW satellite population by a factor of ~ 2 [19].

Our constraint on thermal relic WDM translates to a lower limit of 50 keV on the mass of a non-resonant Dodelson–Widrow sterile neutrino [53, 78]. We also translate our thermal relic WDM limit into constraints on

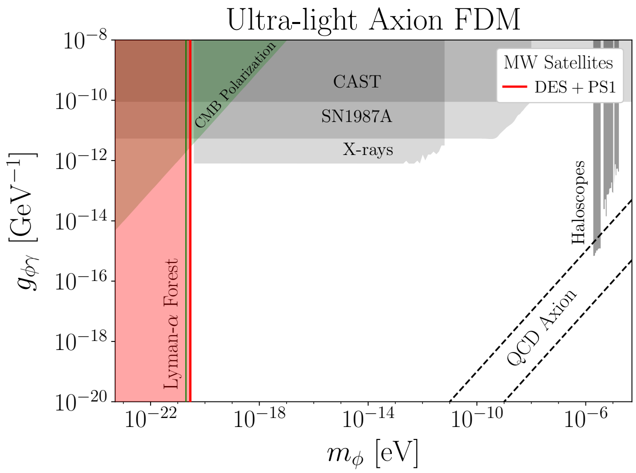

FIG. 3. Constraints on ultra-light axion particle mass versus axion–photon coupling from our analysis of the MW satellite population (red). Limits from CMB polarization washout [72] and the Lyman-α forest [36] are shown in green, and haloscope limits are shown as gray vertical bands. Experimental constraints from the the CAST experiment [73], the lack of a γ-ray signal from SN1987A [74], and the X-ray transparency of the intracluster medium [75] are shown in gray and do not require that the ultra-light axion makes up all of the DM. The dashed lines indicate canoncial QCD axion models [76, 77].

the mass and mixing angle of resonantly-produced sterile neutrinos assuming a Shi–Fuller production mechanism [79], following the conservative procedure described above. As shown in Fig. 2, our analysis rules out nearly the entire remaining parameter space for resonantly produced sterile neutrinos in the Neutrino Minimal Standard Model [66] at greater than 95% confidence. In addition, we robustly rule out the resonantly produced sterile neutrino interpretation of the 3.5 keV X-ray line [61].

(*ii*) *IDM.* Mapping our $m_{\rm WDM} > 6.5\,$keV constraint to the DM–proton scattering model following the procedure in [19] yields constraints on the velocity-independent interaction cross section of $(7.0\times10^{-30}, 2.6\times10^{-29}, 8.8\times10^{-29}, 1.7\times10^{-27})\,\mathrm{cm}^2$ for DM particle masses of $(10^{-5}, 10^{-3}, 10^{-1}, 10)\,$GeV at 95% confidence, as shown in Fig. 2. These constraints scale as $m_\chi^{1/4}$ (m_χ) for $m_\chi \ll 1\,\mathrm{GeV}$ $(m_\chi \gg 1\,\mathrm{GeV})$, and are highly complementary to direction detection limits, particularly at low DM masses [19]. At a DM mass of 100 MeV, our limit translates into an upper bound on the DM–proton coupling of $c_p \lesssim (0.3\,\mathrm{GeV})^{-2}$ [20].

Despite our conservative marginalization over MW halo mass, these results improve upon those in [19] by a factor of ~ 3 at all DM masses. This is stronger than the improvement expected from the analytic prediction for cross section constraints derived in [19] due to a more precise determination of the SHMF, resulting from the sky coverage and sensitivity of DES and PS1.

Several complementary astrophysical and cosmological measurements probe the DM–proton scattering cross section. Stringent limits have been derived by reinterpreting direct detection constraints in the context of cosmic ray upscattering [80]; we do not show these results in Fig. 2 because they constrain the velocity-independent DM–proton cross sections at relativistic energies. The IDM model we consider contributes to the energy density of relativistic species at Big Bang Nucleosynthesis, which sets a lower on its mass that depends on the spin statistics of the DM particle [81–83]. Understanding the interplay of these results with our limits is an important area for future work.

(*iii*) *FDM.* We obtain $M_0 < 1.4\times10^8\,\mathrm{M}_\odot$ at 95% confidence from our fiducial FDM fit. Applying linear MW-host mass scaling yields $M_0 < 1.8\times10^8\,\mathrm{M}_\odot$ at 95% confidence, or $m_\phi > 2.9\times10^{-21}\,$eV. This translates to an upper limit on the de Broglie wavelength of $\lambda_{\rm dB} \lesssim 0.5\ h^{-1}\,$kpc, roughly corresponding to the sizes of the smallest MW satellite galaxies. Thus, the $10^{-22}\,$eV FDM model invoked to solve the core–cusp and too-big-to-fail problems [27], and to fit the internal dynamics of low-surface-brightness [84, 85] and ultra-diffuse [86] galaxies, is strongly disfavored by MW satellite abundances.

To connect to particle models of FDM, we plot this limit in the well-motivated parameter space of ultra-light axion mass versus axion–photon coupling in Fig. 3. For the range of axion–photon couplings that we consider, this mixing has a negligible effect on structure formation. We reiterate that our constraint was derived assuming a light scalar field without self-interactions; this assumption may be violated in specific ultra-light axion models.

Discussion.—In this *Letter*, we used a state-of-the-art model of the MW satellite galaxy population to place stringent and robust limits on three fundamental DM paradigms: WDM, IDM, and FDM. Although some of these alternative DM models gained popularity by solving apparent small-scale structure "challenges" facing CDM, recent observational and theoretical advances have reversed this scenario. In particular, astrophysical and cosmological observations of the smallest DM structures now provide among the strongest constraints on the microphysical properties of DM.

This analysis improves upon previous work by using MW satellite observations over nearly the entire sky, including the population of ultra-faint dwarf galaxies discovered by DES. In addition, our modeling framework rigorously accounts for satellite detectability and uncertainties in the galaxy–halo connection. Our constraints are comparable in sensitivity to Lyman-α forest, strong lensing, and stellar stream perturbation analyses. Future cosmic surveys promise to further improve these measurements [87, 88].

The breadth of DM models constrained by observations of MW satellites is particularly important given the growing interest in a wide range of theoretical possibilities following non-detections in collider, direct, and indirect searches for canonical WIMPs. In addition to the three DM paradigms considered in this work, small-scale structure measurements are also sensitive to the initial DM velocity distribution in non-thermal DM production from scalar field decay [89], the formation redshift of DM in "late–forming" DM models [90], the DM self-interaction cross section [91–94], and the lifetime of decaying DM [95, 96].

Future work could generalize our approach by measuring deviations in the small-scale linear matter power spectrum relative to a baseline CDM scenario, rather than setting constraints in the context of particular DM models. Features in the power spectrum on extremely small scales are a hallmark of many inflationary models [97, 98], and it is conceivable that DM substructure measurements can be used to infer the nature of the corresponding primordial density fluctuations.

Acknowledgements.—This paper has gone through internal review by the DES collaboration. We thank JJ Cherry and Aurel Schneider for providing transfer functions for resonantly-produced sterile neutrinos, and Peter Graham for helpful discussions on ultra-light axions. Our code and subhalo catalogs are available online.[1]

This work was supported in part by U.S. Department of Energy contracts to SLAC (DE-AC02-76SF00515) and Fermilab (DE-AC02-07CH11359). Support was received from the National Science Foundation (NSF) under grant No. NSF AST-1517422, grant No. NSF PHY17-48958 through the Kavli Institute for Theoretical Physics program "The Small-Scale Structure of Cold(?) Dark Matter," and grant No. NSF DGE-1656518 through the NSF Graduate Research Fellowship received by E.O.N. Support for Y.-Y.M. and T.S.L. was provided by NASA through the NASA Hubble Fellowship grant no. HST-HF2-51441.001 awarded by the Space Telescope Science Institute, which is operated by the Association of Universities for Research in Astronomy, Incorporated, under NASA contract NAS5-26555.

This research made use of computational resources at SLAC National Accelerator Laboratory, a U.S. Department of Energy Office of Science laboratory; the authors are thankful for the support of the SLAC computational team. This research made use of the Sherlock cluster at the Stanford Research Computing Center (SRCC); the authors are thankful for the support of the SRCC team. This research made use of `https://arXiv.org` and NASA's Astrophysics Data System for bibliographic information.

Funding for the DES Projects has been provided by the DOE and NSF(USA), MEC/MICINN/MINECO(Spain), STFC(UK), HEFCE(UK). NCSA(UIUC), KICP(U. Chicago), CCAPP(Ohio State), MIFPA(Texas A&M), CNPQ, FAPERJ, FINEP (Brazil), DFG(Germany) and the Collaborating Institutions in DES.

The Collaborating Institutions are Argonne Lab, UC Santa Cruz, University of Cambridge, CIEMAT-Madrid, University of Chicago, University College London, DES-Brazil Consortium, University of Edinburgh, ETH Zürich, Fermilab, University of Illinois, ICE (IEEC-CSIC), IFAE Barcelona, Lawrence Berkeley Lab, LMU München and the associated Excellence Cluster Universe, University of Michigan, NFS's NOIRLab, University of Nottingham, Ohio State University, University of Pennsylvania, University of Portsmouth, SLAC, Stanford University, University of Sussex, Texas A&M University, and the OzDES Membership Consortium.

Based in part on observations at Cerro Tololo Inter-American Observatory at NSFs NOIRLab (NOIRLab Prop. ID 2012B-0001; PI: J. Frieman), which is managed by the Association of Universities for Research in Astronomy (AURA) under a cooperative agreement with the NSF.

The DES Data Management System is supported by the NSF under Grant Numbers AST-1138766 and AST-1536171. The DES participants from Spanish institutions are partially supported by MICINN under grants ESP2017-89838, PGC2018-094773, PGC2018-102021, SEV-2016-0588, SEV-2016-0597, and MDM-2015-0509, some of which include ERDF funds from the European Union. IFAE is partially funded by the CERCA program of the Generalitat de Catalunya. Research leading to these results has received funding from the European Research Council under the European Union's Seventh Framework Program (FP7/2007-2013) including ERC grant agreements 240672, 291329, and 306478. We acknowledge support from the Brazilian Instituto Nacional de Ciência e Tecnologia (INCT) e-Universe (CNPq grant 465376/2014-2).

This manuscript has been authored by Fermi Research Alliance, LLC under Contract No. DE-AC02-07CH11359 with the U.S. Department of Energy, Office of Science, Office of High Energy Physics.

[1] `https://github.com/eonadler/subhalo_satellite_connection`

* enadler@stanford.edu
† kadrlica@fnal.gov
‡ NHFP Einstein Fellow

[1] N. Aghanim, Y. Akrami, M. Ashdown, J. Aumont, C. Baccigalupi, M. Ballardini, A. J. Banday, R. B. Barreiro, N. Bartolo, S. Basak, et al. (Planck Collaboration), arXiv e-prints (2018), 1807.06209.

[2] R. D. Peccei and H. R. Quinn, Phys. Rev. Lett. **38**, 1440 (1977).

[3] G. Jungman, M. Kamionkowski, and K. Griest, Phys. Rep. **267**, 195 (1996), hep-ph/9506380.
[4] G. Bertone, D. Hooper, and J. Silk, Phys. Rep. **405**, 279 (2005), hep-ph/0404175.
[5] J. S. Bullock and M. Boylan-Kolchin, ARA&A **55**, 343 (2017), 1707.04256.
[6] M. R. Buckley and A. H. G. Peter, Phys. Rep. **761**, 1 (2018), 1712.06615.
[7] J. D. Simon, ARA&A **57**, 375 (2019), 1901.05465.
[8] J. S. Bullock, A. V. Kravtsov, and D. H. Weinberg, ApJ **539**, 517 (2000), astro-ph/0002214.
[9] A. V. Macciò and F. Fontanot, MNRAS **404**, L16 (2010), 0910.2460.
[10] E. Polisensky and M. Ricotti, Phys. Rev. D **83**, 043506 (2011), 1004.1459.
[11] D. Anderhalden, A. Schneider, A. V. Macciò, J. Diemand, and G. Bertone, J. Cosmology Astropart. Phys. **2013**, 014 (2013), 1212.2967.
[12] K. N. Abazajian, Phys. Rev. Lett. **112**, 161303 (2014), 1403.0954.
[13] M. R. Lovell, C. S. Frenk, V. R. Eke, A. Jenkins, L. Gao, and T. Theuns, MNRAS **439**, 300 (2014), 1308.1399.
[14] R. Kennedy, C. Frenk, S. Cole, and A. Benson, MNRAS **442**, 2487 (2014), 1310.7739.
[15] K. N. Abazajian, Phys. Rep. **711**, 1 (2017), 1705.01837.
[16] R. Adhikari, M. Agostini, N. A. Ky, T. Araki, M. Archidiacono, M. Bahr, J. Baur, J. Behrens, F. Bezrukov, P. S. Bhupal Dev, et al., J. Cosmology Astropart. Phys. **2017**, 025 (2017), 1602.04816.
[17] C. Bœhm, P. Fayet, and R. Schaeffer, Physics Letters B **518**, 8 (2001), astro-ph/0012504.
[18] C. Boehm and R. Schaeffer, A&A **438**, 419 (2005), astro-ph/0410591.
[19] E. O. Nadler, V. Gluscevic, K. K. Boddy, and R. H. Wechsler, ApJ **878**, L32 (2019), 1904.10000.
[20] K. K. Boddy and V. Gluscevic, Phys. Rev. D **98**, 083510 (2018), 1801.08609.
[21] K. K. Boddy, V. Gluscevic, V. Poulin, E. D. Kovetz, M. Kamionkowski, and R. Barkana, Phys. Rev. D **98**, 123506 (2018), 1808.00001.
[22] V. Gluscevic and K. K. Boddy, Phys. Rev. Lett. **121**, 081301 (2018).
[23] C. Boehm, J. A. Schewtschenko, R. J. Wilkinson, C. M. Baugh, and S. Pascoli, MNRAS **445**, L31 (2014), 1404.7012.
[24] J. A. Schewtschenko, C. M. Baugh, R. J. Wilkinson, C. Bœhm, S. Pascoli, and T. Sawala, MNRAS **461**, 2282 (2016), 1512.06774.
[25] M. Escudero, L. Lopez-Honorez, O. Mena, S. Palomares-Ruiz, and P. Villanueva-Domingo, J. Cosmology Astropart. Phys. **2018**, 007 (2018), 1803.08427.
[26] W. Hu, R. Barkana, and A. Gruzinov, Phys. Rev. Lett. **85**, 1158 (2000), astro-ph/0003365.
[27] L. Hui, J. P. Ostriker, S. Tremaine, and E. Witten, Phys. Rev. D **95**, 043541 (2017), 1610.08297.
[28] X. Du, Ph.D. thesis, Gottingen U. (2019).
[29] D. J. E. Marsh, Phys. Rep. **643**, 1 (2016), 1510.07633.
[30] A. Drlica-Wagner, K. Bechtol, S. Mau, M. McNanna, E. O. Nadler, A. B. Pace, T. S. Li, A. Pieres, E. Rozo, J. D. Simon, et al. (DES Collaboration), ApJ **893**, 47 (2020), 1912.03302.
[31] DES Collaboration, T. M. C. Abbott, F. B. Abdalla, S. Allam, et al., ApJS **239**, 18 (2018), 1801.03181.
[32] K. C. Chambers, E. A. Magnier, N. Metcalfe, H. A. Flewelling, M. E. Huber, C. Z. Waters, L. Denneau, P. W. Draper, D. Farrow, D. P. Finkbeiner, et al., ArXiv e-prints (2016), 1612.05560.
[33] E. O. Nadler, R. H. Wechsler, K. Bechtol, Y. Y. Mao, G. Green, A. Drlica-Wagner, M. McNanna, S. Mau, A. B. Pace, J. D. Simon, et al. (DES Collaboration), ApJ **893**, 48 (2020), 1912.03303.
[34] M. Viel, G. D. Becker, J. S. Bolton, and M. G. Haehnelt, Phys. Rev. D **88**, 043502 (2013), 1306.2314.
[35] V. Iršič, M. Viel, M. G. Haehnelt, J. S. Bolton, S. Cristiani, G. D. Becker, V. D'Odorico, G. Cupani, T.-S. Kim, T. A. M. Berg, et al., Phys. Rev. D **96**, 023522 (2017), 1702.01764.
[36] V. Iršič, M. Viel, M. G. Haehnelt, J. S. Bolton, and G. D. Becker, Phys. Rev. Lett. **119**, 031302 (2017), 1703.04683.
[37] J. W. Hsueh, W. Enzi, S. Vegetti, M. W. Auger, C. D. Fassnacht, G. Despali, L. V. E. Koopmans, and J. P. McKean, MNRAS **492**, 3047 (2020), 1905.04182.
[38] D. Gilman, S. Birrer, A. Nierenberg, T. Treu, X. Du, and A. Benson, MNRAS **491**, 6077 (2020), 1908.06983.
[39] N. Banik, J. Bovy, G. Bertone, D. Erkal, and T. J. L. de Boer, arXiv e-prints arXiv:1911.02663 (2019), 1911.02663.
[40] S. Y. Kim, A. H. G. Peter, and J. R. Hargis, Phys. Rev. Lett. **121**, 211302 (2018).
[41] G. Hinshaw, D. Larson, E. Komatsu, D. N. Spergel, C. L. Bennett, J. Dunkley, M. R. Nolta, M. Halpern, R. S. Hill, N. Odegard, et al., ApJS **208**, 19 (2013).
[42] P. Bode, J. P. Ostriker, and N. Turok, ApJ **556**, 93 (2001), astro-ph/0010389.
[43] A. Schneider, R. E. Smith, A. V. Macciò, and B. Moore, MNRAS **424**, 684 (2012), 1112.0330.
[44] G. L. Bryan and M. L. Norman, ApJ **495**, 80 (1998), astro-ph/9710107.
[45] Y.-Y. Mao, M. Williamson, and R. H. Wechsler, ApJ **810**, 21 (2015), 1503.02637.
[46] P. Jethwa, D. Erkal, and V. Belokurov, MNRAS **473**, 2060 (2018), 1612.07834.
[47] M. R. Lovell, C. S. Frenk, V. R. Eke, A. Jenkins, L. Gao, and T. Theuns, MNRAS **439**, 300 (2014), 1308.1399.
[48] S. Bose, W. A. Hellwing, C. S. Frenk, A. Jenkins, M. R. Lovell, J. C. Helly, B. Li, V. Gonzalez-Perez, and L. Gao, MNRAS **464**, 4520 (2017), 1604.07409.
[49] L. Lancaster, C. Giovanetti, P. Mocz, Y. Kahn, M. Lisanti, and D. N. Spergel, J. Cosmology Astropart. Phys. **2020**, 001 (2020), 1909.06381.
[50] E. O. Nadler, Y.-Y. Mao, G. M. Green, and R. H. Wechsler, ApJ **873**, 34 (2019), 1809.05542.
[51] D. Foreman-Mackey, D. W. Hogg, D. Lang, and J. Goodman, PASP **125**, 306 (2013), 1202.3665.
[52] T. M. Callingham, M. Cautun, A. J. Deason, C. S. Frenk, W. Wang, F. A. Gómez, R. J. J. Grand, F. Marinacci, and R. Pakmor, MNRAS **484**, 5453 (2019), 1808.10456.
[53] M. Viel, J. Lesgourgues, M. G. Haehnelt, S. Matarrese, and A. Riotto, Phys. Rev. D **71**, 063534 (2005), astro-ph/0501562.
[54] M. R. Lovell, MNRAS **493**, L11 (2020), 1911.11785.
[55] R. E. Angulo, O. Hahn, and T. Abel, MNRAS **434**, 3337 (2013), 1304.2406.
[56] J. Wang and S. D. M. White, MNRAS **380**, 93 (2007), astro-ph/0702575.
[57] M. R. Lovell, ApJ **897**, 147 (2020), 2003.01125.
[58] A. Schneider, J. Cosmology Astropart. Phys. **2016**, 059 (2016), 1601.07553.

[59] K. Maamari, K. K. Boddy, V. Gluscevic, E. O. Nadler, and R. H. Wechsler, in prep. (2020).
[60] J. F. Cherry and S. Horiuchi, Phys. Rev. D **95**, 083015 (2017), 1701.07874.
[61] A. Boyarsky, O. Ruchayskiy, D. Iakubovskyi, and J. Franse, Phys. Rev. Lett. **113**, 251301 (2014), 1402.4119.
[62] A. Boyarsky, O. Ruchayskiy, and D. Iakubovskyi, J. Cosmology Astropart. Phys. **2009**, 005 (2009), 0808.3902.
[63] S. Horiuchi, P. J. Humphrey, J. Oñorbe, K. N. Abazajian, M. Kaplinghat, and S. Garrison-Kimmel, Phys. Rev. D **89**, 025017 (2014), 1311.0282.
[64] K. Perez, K. C. Y. Ng, J. F. Beacom, C. Hersh, S. Horiuchi, and R. Krivonos, Phys. Rev. D **95**, 123002 (2017), 1609.00667.
[65] C. Dessert, N. L. Rodd, and B. R. Safdi, Science **367**, arXiv:1812.06976 (2020), 1812.06976.
[66] T. Asaka, S. Blanchet, and M. Shaposhnikov, Physics Letters B **631**, 151 (2005), hep-ph/0503065.
[67] W. L. Xu, C. Dvorkin, and A. Chael, Phys. Rev. D **97**, 103530 (2018).
[68] M. S. Mahdawi and G. R. Farrar, J. Cosmology Astropart. Phys. **2018**, 007 (2018), 1804.03073.
[69] T. Emken and C. Kouvaris, Phys. Rev. D **97**, 115047 (2018).
[70] H.-Y. Schive, T. Chiueh, T. Broadhurst, and K.-W. Huang, ApJ **818**, 89 (2016), 1508.04621.
[71] K. Schutz, Phys. Rev. D **101**, 123026 (2020).
[72] M. A. Fedderke, P. W. Graham, and S. Rajendran, Phys. Rev. D **100**, 015040 (2019), 1903.02666.
[73] M. Arik, S. Aune, K. Barth, A. Belov, H. Bräuninger, J. Bremer, V. Burwitz, G. Cantatore, J. M. Carmona, S. A. Cetin, et al., Phys. Rev. D **92**, 021101 (2015), 1503.00610.
[74] A. Payez, C. Evoli, T. Fischer, M. Giannotti, A. Mirizzi, and A. Ringwald, J. Cosmology Astropart. Phys. **2015**, 006 (2015), 1410.3747.
[75] C. S. Reynolds, M. C. D. Marsh, H. R. Russell, A. C. Fabian, R. Smith, F. Tombesi, and S. Veilleux, ApJ **890**, 59 (2020), 1907.05475.
[76] J. E. Kim, Phys. Rev. Lett. **43**, 103 (1979).
[77] M. Dine, W. Fischler, and M. Srednicki, Physics Letters B **104**, 199 (1981).
[78] S. Dodelson and L. M. Widrow, Phys. Rev. Lett. **72**, 17 (1994), hep-ph/9303287.
[79] X. Shi and G. M. Fuller, Phys. Rev. Lett. **82**, 2832 (1999).
[80] T. Bringmann and M. Pospelov, Phys. Rev. Lett. **122**, 171801 (2019).
[81] C. Bœhm, M. J. Dolan, and C. McCabe, J. Cosmology Astropart. Phys. **2013**, 041 (2013), 1303.6270.
[82] K. M. Nollett and G. Steigman, Phys. Rev. D **91**, 083505 (2015), 1411.6005.
[83] G. Krnjaic and S. D. McDermott, Phys. Rev. D **101**, 123022 (2020), 1908.00007.
[84] T. Bernal, L. M. Fernndez-Hernndez, T. Matos, and M. A. Rodrguez-Meza, MNRAS **475**, 1447 (2017), 1701.00912.
[85] T. Broadhurst, I. De Martino, H. N. Luu, G. F. Smoot, and S.-H. H. Tye, Phys. Rev. D **101**, 083012 (2020).
[86] A. Wasserman, P. van Dokkum, A. J. Romanowsky, J. Brodie, S. Danieli, D. A. Forbes, R. Abraham, C. Martin, M. Matuszewski, A. Villaume, et al., ApJ **885**, 155 (2019), 1905.10373.
[87] A. Drlica-Wagner, Y.-Y. Mao, S. Adhikari, R. Armstrong, A. Banerjee, N. Banik, K. Bechtol, S. Bird, K. K. Boddy, A. Bonaca, et al., arXiv e-prints arXiv:1902.01055 (2019), 1902.01055.
[88] The MSE Science Team, C. Babusiaux, M. Bergemann, A. Burgasser, S. Ellison, D. Haggard, D. Huber, M. Kaplinghat, T. Li, J. Marshall, et al., arXiv e-prints arXiv:1904.04907 (2019), 1904.04907.
[89] C. Miller, A. L. Erickcek, and R. Murgia, Phys. Rev. D **100**, 123520 (2019), 1908.10369.
[90] A. Sarkar, S. Das, and S. K. Sethi, J. Cosmology Astropart. Phys. **2015**, 004 (2015), 1410.7129.
[91] M. Vogelsberger, J. Zavala, and A. Loeb, MNRAS **423**, 3740 (2012), 1201.5892.
[92] J. Zavala, M. Vogelsberger, and M. G. Walker, MNRAS **431**, L20 (2013), 1211.6426.
[93] S. Tulin and H.-B. Yu, Phys. Rep. **730**, 1 (2018), 1705.02358.
[94] E. O. Nadler, A. Banerjee, S. Adhikari, Y.-Y. Mao, and R. H. Wechsler, ApJ **896**, 112 (2020), 2001.08754.
[95] A. H. G. Peter, C. E. Moody, and M. Kamionkowski, Phys. Rev. D **81**, 103501 (2010), 1003.0419.
[96] M.-Y. Wang, A. H. G. Peter, L. E. Strigari, A. R. Zentner, B. Arant, S. Garrison-Kimmel, and M. Rocha, MNRAS **445**, 614 (2014), 1406.0527.
[97] M. Kamionkowski and A. R. Liddle, Phys. Rev. Lett. **84**, 4525 (2000), astro-ph/9911103.
[98] M. White and R. A. C. Croft, ApJ **539**, 497 (2000), astro-ph/0001247.
[99] S. R. Hinton, JOSS **1**, 00045 (2016).

Parameter	Physical Interpretation	95% confidence interval
α	Power-law slope of satellite luminosity function	$-1.46 < \alpha < -1.38$
σ_M	Scatter in satellite luminosity at fixed halo properties	$0\ \mathrm{dex}^* < \sigma_M < 0.2\ \mathrm{dex}$
$\mathcal{M}_{50}$	Peak mass at which 50% of halos host galaxies	$7.5^* < \log(\mathcal{M}_{50}/\,\mathrm{M}_\odot) < 8.0$
$\mathcal{B}$	Subhalo disruption efficiency relative to FIRE simulations	$0.2 < \mathcal{B} < 1.9$
$\sigma_{\rm gal}$	Width of the galaxy occupation fraction	$0\ \mathrm{dex}^* < \sigma_M < 0.66\ \mathrm{dex}$
$\mathcal{A}$	Amplitude of relation between galaxy size and halo size	$0\,\mathrm{pc}^* < \mathcal{A} < 90\,\mathrm{pc}$
$\sigma_{\log R}$	Scatter in galaxy size at fixed halo properties	$0.1\ \mathrm{dex}^* < \sigma_M < 1.1\ \mathrm{dex}$
n	Power-law slope of relation between galaxy size and halo size	$0^* < n < 1.9$
$M_{\rm hm}$	Mass scale of thermal relic WDM SHMF suppression (Eq. (5))	$7.0^* < \log(\mathcal{M}_{\rm hm}/\,\mathrm{M}_\odot) < 7.5$
M_0	Mass scale of FDM SHMF suppression (Eq. (7))	$7.0^* < \log(\mathcal{M}_0/\,\mathrm{M}_\odot) < 8.1$

TABLE II. Galaxy–halo connection and DM model parameters varied in our thermal relic WDM and FDM fits to the MW satellite population. Note that M_0 is constrained in a separate fit that yields similar confidence intervals for the eight galaxy–halo connection parameters. Asterisks mark prior-driven constraints. See [33] for details on our galaxy–halo connection model.

SUPPLEMENTAL MATERIAL

Fitting Procedure Details and Posterior Distributions

Our DM limits are derived by running 10^5 iterations of the MCMC sampler `emcee` [51] to sample the eight galaxy–halo connection model parameters described in [33], plus the DM model parameter of interest (i.e., $M_{\rm hm}$ for our thermal relic WDM fit and M_0 for our FDM fit), using 36 walkers. The eight galaxy–halo connection model parameters are shown in Table II and described in detail by [33]. For both our thermal relic WDM and FDM fits, we discard a generous burn-in period of 2×10^4 steps, corresponding to ~ 20 autocorrelation lengths. We use the Python package `ChainConsumer` [99] to visualize the posterior distributions and calculate confidence intervals.

The posterior distributions over galaxy–halo connection and DM model parameters for our thermal relic WDM and FDM analyses are shown in Fig. 4 and Fig. 5, respectively. Our IDM constraints are derived using the $M_{\rm hm}$ limit from our thermal relic WDM fit; thus, we do not show a separate posterior for the IDM analysis.

Resonantly-Produced Sterile Neutrino Constraints

To translate our upper bound on the mass of thermal relic WDM into constraints on resonantly-produced Shi–Fuller sterile neutrinos, we follow the procedure in [58, 59]. In particular, we use the sterile neutrino transfer functions generated by [60] using `CLASS` for a grid of sterile neutrino masses and mixing angles. We then compare these transfer functions to the $m_{\rm WDM} = 6.5\,\mathrm{keV}$ thermal relic transfer function that is ruled out at 95% confidence by our analysis. We derive the limits in Fig. 2 by finding the combinations of sterile neutrino mass and mixing angle between the "DM Underproduction" and "DM Overproduction" lines in Fig. 2 that yield transfer functions which are strictly more suppressed than the ruled-out thermal relic transfer function. The overproduction (underproduction) boundaries correspond to sterile neutrino models with zero (maximal) lepton asymmetry in the Neutrino Minimal Standard Model [58].

We benchmark our sterile neutrino limits using the recent estimate of SHMF suppression from [57], which is appropriate for a 7 keV resonantly-produced sterile neutrino with various lepton asymmetry (or mixing angle) values. This SHMF suppression corresponds to Eq. (4) with $\alpha = 4.2$, $\beta = 2.5$, $\gamma = -0.2$, and the relation between $M_{\rm hm}$ and lepton asymmetry L_6 is given for several models in [57]. Using this SHMF in our fitting procedure, we find $M_{\rm hm} < 5.9 \times 10^7\ \mathrm{M}_\odot$ at 95% confidence. Applying linear scaling with MW halo mass to the result of the joint fit yields $M_{\rm hm} < 7.6 \times 10^7\,\mathrm{M}_\odot$, which rules out the coldest sterile neutrino model presented in [57]—corresponding to $m_s = 7\,\mathrm{keV}$ and $L_6 = 8$—at $\gg 95\%$ confidence, consistent with our limit in Fig. 2.

FDM Subhalo Mass Functions

Due to the difficulties of simulating non-linear structure formation in FDM, no consensus exists for a quantitative description of the suppression of the SHMF in this model. We therefore implemented two popular forms of the FDM

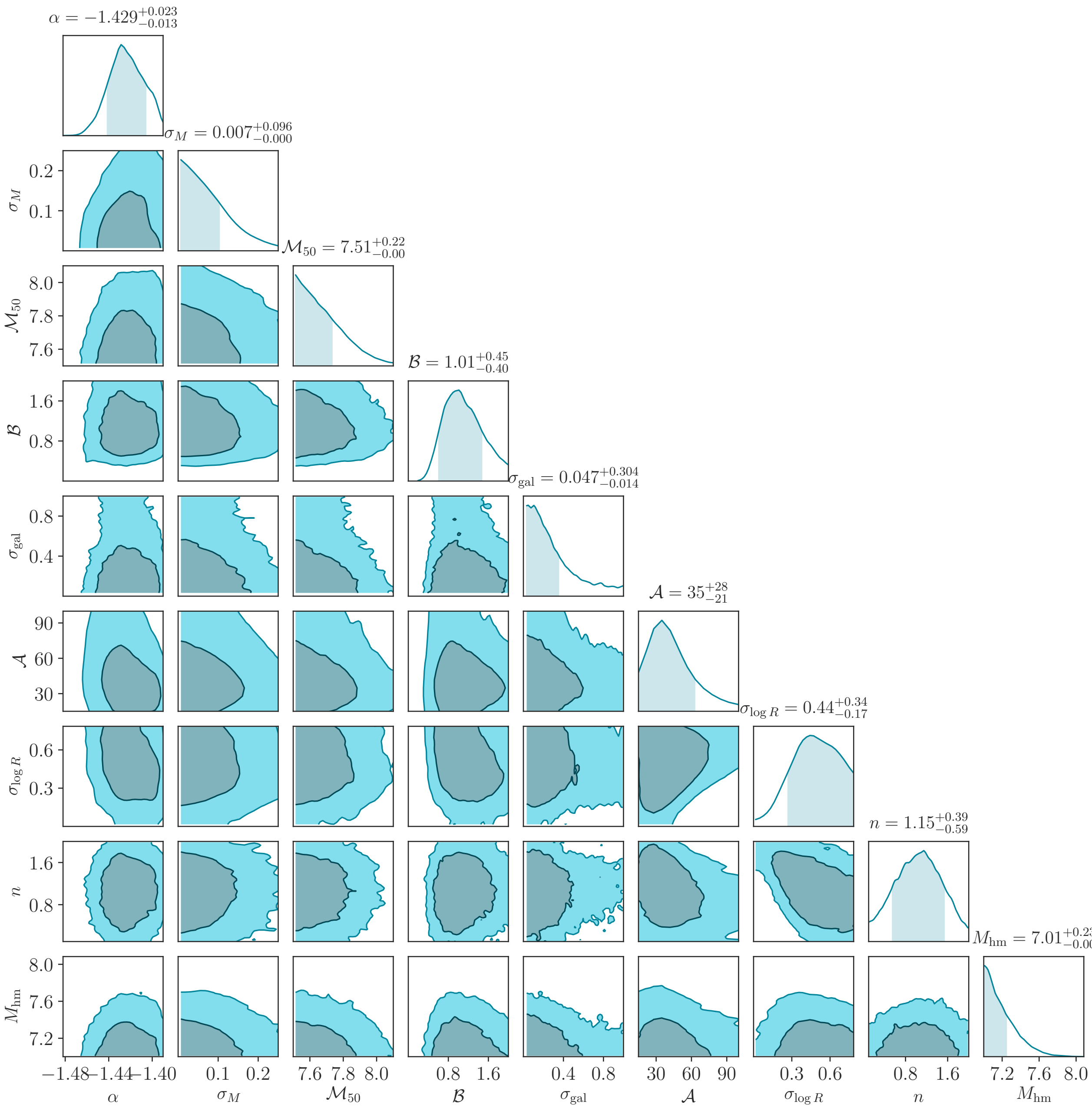

FIG. 4. Posterior distribution from our fit to the DES and PS1 satellite populations for thermal relic WDM. Dark (light) shaded contours represent 68% (95%) confidence intervals. Shaded areas in the marginal distributions and parameter summaries correspond to 68% confidence intervals. Note that σ_M, $\sigma_{\rm gal}$, and $\sigma_{\log R}$ are reported in dex, $\mathcal{M}_{50}$ and $M_{\rm hm}$ are reported as $\log(\mathcal{M}_{50}/\,{\rm M}_\odot)$ and $\log(M_{\rm hm}/\,{\rm M}_\odot)$, $\mathcal{A}$ is reported in pc, and α, $\mathcal{B}$, and n are dimensionless.

SHMF to assess this uncertainty. The nominal model described in the text is the semi-analytic model derived in [28]. Our fit to this function is given by Eq. (6), with

$$\tilde{\beta}(m_\phi) = \exp\left[-\left(\frac{m_\phi}{13.7\times 10^{-22}\,{\rm eV}}\right)^{0.6}\right] + 0.77 \tag{8}$$

$$\tilde{\gamma}(m_\phi) = 0.22\log\left[\left(\frac{m_\phi}{10^{-22}\,{\rm eV}}\right)^{0.45}\right] - 0.78. \tag{9}$$

An alternative model for the suppression of the halo mass function is derived from the "wave dark matter" simulations in [70], which corresponds to Eq. (6) with $\tilde{\beta} = 1.1$ and $\tilde{\gamma} = -2.2$. This mass function was estimated using

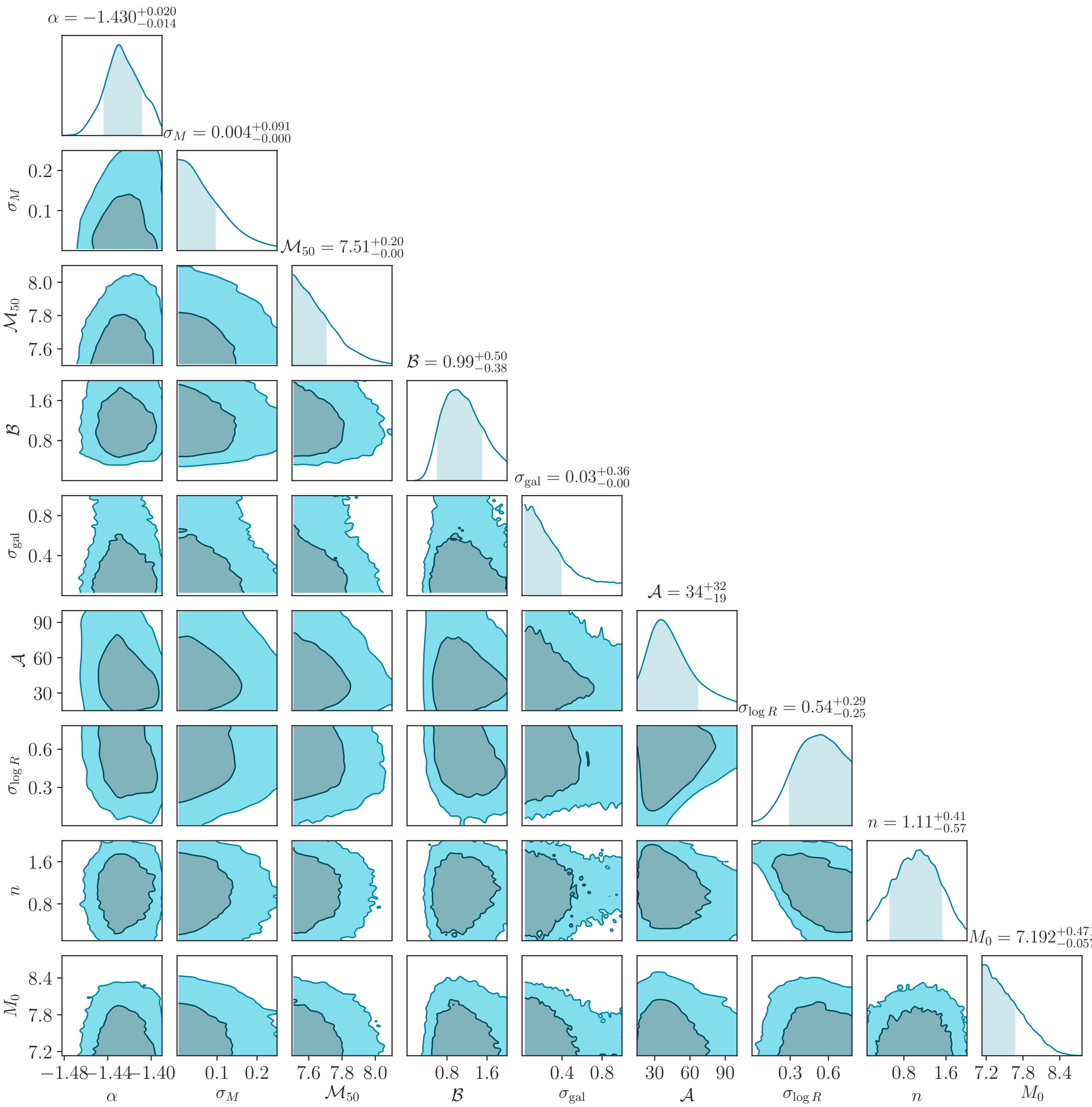

FIG. 5. Same as Fig. 4, but for our FDM fit.

high-redshift ($z > 4$) simulation outputs and is systematically more suppressed than that derived semi-analytically in [28]. Adopting this alternative SHMF in our fitting procedure and accounting for the uncertainty in MW halo mass yields $M_0 < 3.4 \times 10^7\ \mathrm{M}_\odot$ at 95% confidence, corresponding to $m_\phi > 9.1 \times 10^{-21}$ eV. Thus, the current FDM SHMF uncertainty results in roughly a factor of three difference relative to our fiducial $m_\phi > 2.9 \times 10^{-21}$ eV constraint.

We caution that these uncertainties underlie FDM predictions from *both* semi-analytic models and simulations. For example, [70] simulate CDM-like particles with initial conditions appropriate for FDM, and thus do not solve the Schrödinger–Poisson system that governs FDM. This is an important caveat, because interference patterns on scales comparable to the de Broglie wavelength can potentially affect structure formation. Meanwhile, the semi-analytic treatment in [28] does not explicitly account for the "quantum pressure" term in the Madelung transformation of the Schrödinger–Poisson system, and makes several assumptions about the tidal evolution of subhalos with solitonic density profiles. The derivation of robust, quantitative predictions for the FDM SHMF represents an active area of theoretical and computational study.